nature portfolio

https://doi.org/10.1038/s41586-022-05088-z

Supplementary information

An elementary quantum network of entangled optical atomic clocks

In the format provided by the authors and unedited

Supplementary Information: An elementary quantum network of entangled optical atomic clocks

B. C. Nichol*, R. Srinivas*, D. P. Nadlinger, P. Drmota, D. Main, G. Araneda, C. J. Ballance, and D. M. Lucas
Department of Physics, University of Oxford, Clarendon Laboratory, Parks Road, Oxford OX1 3PU, U.K.
(Dated: 16/06/2022)

A. Mapping remote entanglement to optical qubit

The initial entanglement is generated using the $|S_{1/2}, m_J = \pm 1/2\rangle$ states that are separated by 14 MHz[19]. To generate this entaglement, we first excite both atoms simultaneously to the $|P_{1/2}, m_J = +1/2\rangle$ state using a fast pulse from a 422 nm picosecond laser. The spontaneously emitted 422 nm photons, whose polarisations are entangled with the internal state of the ions, are collected in single-mode optical fibres. The fibres transmit these photons to a Bell-state analyser, where measurements conditioned on the photon polarisations project the ions into an entangled state. To map this entanglement to the optical qubit on each atom, we use a π-pulse on the $|S_{1/2}, m_J = +1/2\rangle \leftrightarrow |D_{5/2}, m_J = -3/2\rangle$ transition. This sequence creates the entangled Bell state

$$|\Psi\rangle = \frac{1}{\sqrt{2}}(|\downarrow\uparrow\rangle \pm e^{i\phi}|\uparrow\downarrow\rangle), \tag{S1}$$

where $|\downarrow\rangle \equiv |S_{1/2}, m_j = -1/2\rangle$, and $|\uparrow\rangle \equiv |D_{5/2}, m_j = -3/2\rangle$.

B. Bell-state phase calibration

We measure the frequency difference between the atoms $\Delta_- = \Delta_1 - \Delta_2 = \omega_2 - \omega_1$, where $\Delta_i = \omega_L - \omega_i$. The laser and atomic frequencies are denoted by ω_L and ω_i respectively. To measure Δ_- using entangled atoms, we require the state $|\Psi\rangle = \frac{1}{\sqrt{2}}(|\downarrow\uparrow\rangle \pm e^{i\phi}|\uparrow\downarrow\rangle)$. Entanglement can also improve measurements of $\Delta_+ = \Delta_1 + \Delta_2$, which can be used to stabilise the laser frequency to the mean atomic frequency; this measurement requires the entangled state $|\Phi\rangle = \frac{1}{\sqrt{2}}(|\downarrow\downarrow\rangle \pm e^{i\phi'}|\uparrow\uparrow\rangle)$.

We initially create the entangled state $|\Psi\rangle = \frac{1}{\sqrt{2}}(|\downarrow\uparrow\rangle \pm e^{i\phi}|\uparrow\downarrow\rangle)$, where ϕ is set by optical paths in the apparatus, and $\pm$ corresponds to the specific detector pattern in the Bell state analyser that heralds entanglement[19]. To remain in the optimal entangled state for measuring Δ_-, we adjust the phase of the Ramsey experiment (ϕ_0 in Fig 1b) in Alice with respect to that in Bob to be $\phi_0 = \phi + \pi$. Sample calibration data is shown in Fig. S1, where we determine the optimal ϕ_0 required for each of the 4 possible valid detector patterns. This phase is updated in real time within the experimental sequence to acquire data from all heralds. Figure S2 shows the parity contrast versus time for the single-ion measurements, the two-ion unentangled state and the two-ion entangled state $|\Psi\rangle$. By setting $\phi_0 = \phi$, we can transform $|\Psi\rangle$ to $|\Phi\rangle$. We also performed Ramsey experiments using $|\Phi\rangle$ as shown in Fig. S3. As $|\Phi\rangle$ is symmetric, we set $\phi_2 = \phi_1$ and scanned ϕ_1 for these data. This state has a faster decay in contrast due to increased sensitivity to laser dephasing.

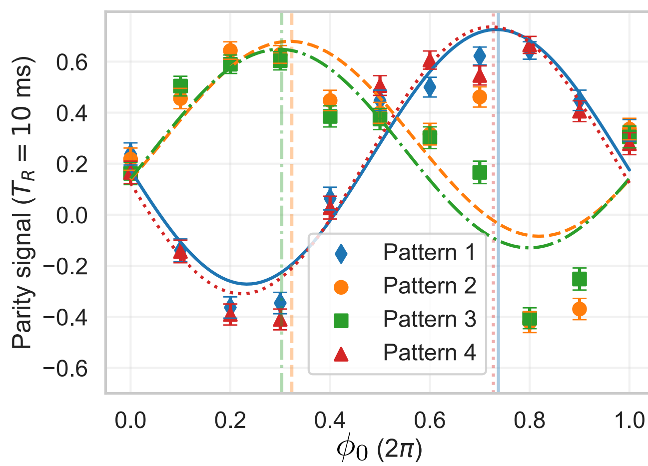

FIG. S1: Calibration of ϕ_0, the relative phase of the Ramsey experiments in Alice with respect to Bob. For a Ramsey duration of 10 ms, and fixed analysis phases ϕ_1 and ϕ_2, we plot the two-ion parity versus ϕ_0 for each of the 4 detector patterns in the Bell state analyser[19]. The optimal ϕ_0 corresponds to the peak of the parity signal (vertical lines). Patterns 1 (blue diamonds) and 4 (red triangles) are approximately π radians out of phase from patterns 2 (orange circles) and 3 (green squares), corresponding to the phase offset of the resulting entangled state.

C. Echo sequence

We alternate between the optical transitions $|\downarrow\rangle \equiv |S_{1/2}, m_j = -1/2\rangle \leftrightarrow |\uparrow\rangle \equiv |D_{5/2}, m_j = -3/2\rangle$ and $|\downarrow'\rangle \equiv |S_{1/2}, m_j = +1/2\rangle \leftrightarrow |\uparrow'\rangle \equiv |D_{5/2}, m_j = +3/2\rangle$, which have magnetic field sensitivities of -11.2 MHz/mT and $+11.2$ MHz/mT, respectively. Thus, by alternating between these transitions, we can 'echo out' slow qubit frequency drifts due to fluctuations in the magnetic field, while still measuring a shift of the centre-of-gravity of the 674 nm

*These authors contributed equally.
Email:bethan.nichol@physics.ox.ac.uk,
raghavendra.srinivas@physics.ox.ac.uk

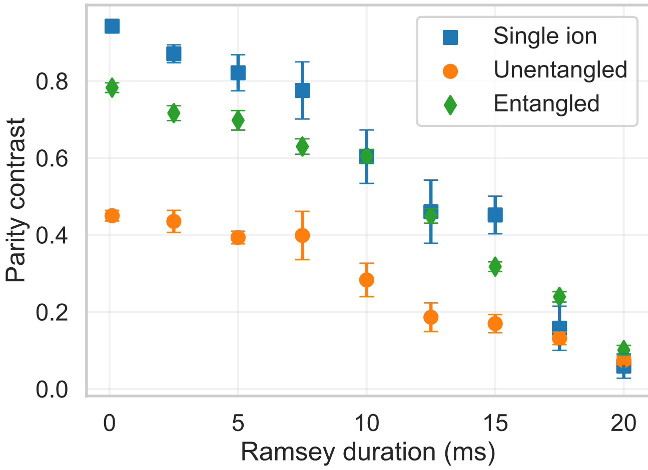

FIG. S2: Parity contrast versus Ramsey duration. For each Ramsey duration, we perform phase scans as shown in Fig. 2 and measure the contrast. The single-ion measurements are the average contrast from Alice and Bob. For single-ion (blue squares), unentangled (orange circles), and entangled (green diamonds) measurements, the contrast decays due to qubit decoherence. The contrast for the single-ion measurements also decays due to laser dephasing.

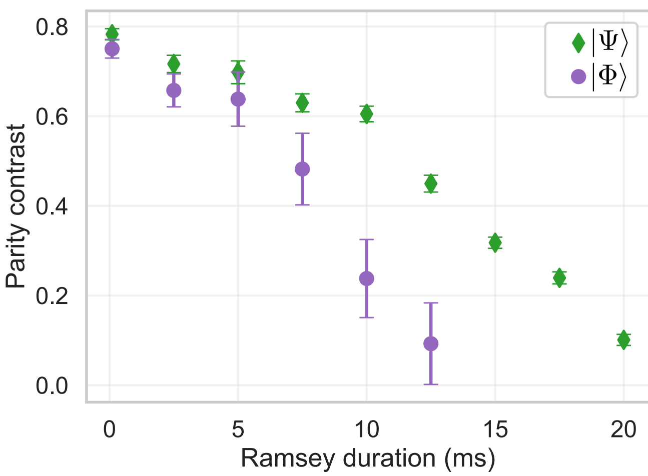

FIG. S3: Two-ion parity contrast versus Ramsey duration for $|\Psi\rangle = \frac{1}{\sqrt{2}}(|\downarrow\uparrow\rangle \pm e^{i\phi}|\uparrow\downarrow\rangle)$ and $|\Phi\rangle = \frac{1}{\sqrt{2}}(|\downarrow\downarrow\rangle \pm e^{i\phi'}|\uparrow\uparrow\rangle)$. Compared to $|\Psi\rangle$ (green diamonds), $|\Phi\rangle$ (purple circles) has a faster decay in contrast due to an increased sensitivity to laser dephasing. All error bars indicate 68% confidence intervals.

transition. To map $|\uparrow\rangle \to |\uparrow'\rangle$ and $|\downarrow\rangle \to |\downarrow'\rangle$, we perform the following echo sequence using 674 nm π-pulses resonant with the required transition, as illustrated in Fig. S4:

1. $|\uparrow\rangle \equiv |D_{5/2}, m_j = -3/2\rangle \to |S_{1/2}, m_j = +1/2\rangle$
2. $|S_{1/2}, m_j = +1/2\rangle \to |D_{5/2}, m_j = +3/2\rangle \equiv |\uparrow'\rangle$
3. $|\downarrow\rangle \equiv |S_{1/2}, m_j = -1/2\rangle \to |D_{5/2}, m_j = -3/2\rangle$
4. $|D_{5/2}, m_j = -3/2\rangle \to |S_{1/2}, m_j = +1/2\rangle \equiv |\downarrow'\rangle$

The total duration of this pulse sequence is $\approx 44\,\mu$s. To map $|\downarrow'\rangle \to |\downarrow\rangle$ and $|\uparrow'\rangle \to |\uparrow\rangle$, we perform the same sequence in reverse order. For the experiments described in the main text, we perform a total of 5 such sequences to achieve Walsh-7 modulation[57]. The Ramsey duration T_R excludes the length of these echo sequences. The choice of Walsh sequence index depends on the magnetic field noise spectrum; for our system, the Walsh-7 sequence optimally increased the coherence time without significantly reducing the contrast due to imperfect π-pulses, as shown in Fig. S5. For single qubit-rotations, we observe an error of $\sim 5\times10^{-4}$. This error increases to $\sim 3\times10^{-3}$ for the entangled state due to heating of the ions during the entanglement-attempt sequence.

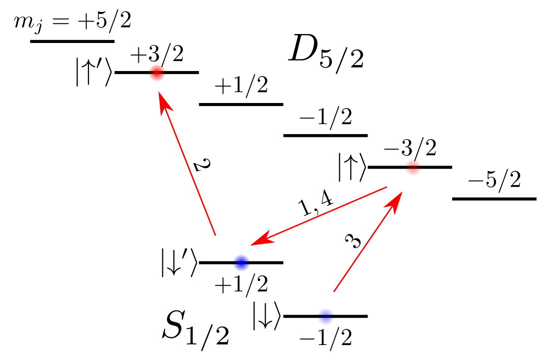

FIG. S4: Modified spin-echo sequence. We map the $|\downarrow\rangle$ and $|\uparrow\rangle$ qubit states to the $|\downarrow'\rangle$ and $|\uparrow'\rangle$ states following the pulse sequence described in the text. The primed states have equal and opposite magnetic field sensitivities to the unprimed states.

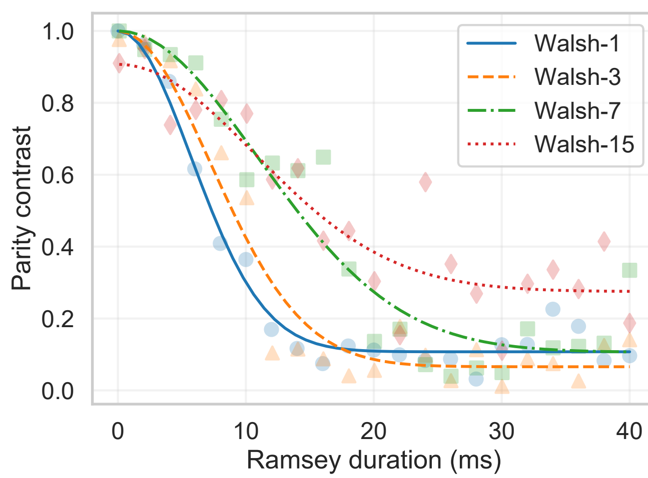

FIG. S5: Single-ion parity contrast versus Ramsey duration for different Walsh sequence indices 1 (blue circles), 3 (orange triangles), 7 (green squares), and 15 (red diamonds). As we increase the Walsh sequence index, we observe higher contrasts at longer durations. We fit a Gaussian decay to each dataset. For the experiments described in the main text, we use a Walsh-7 sequence.

D. Magnetic field stabilisation

The two primary sources of magnetic-field noise are fluctuations in the current supplied to the coils, and ambient AC fields at 50 Hz (and harmonics) induced by wires carrying mains current in the vicinity of the traps. Stabilisation circuits[58] on the magnetic field coils reduce these noise sources and increase the coherence time of the optical $^{88}Sr^+$ qubit from 0.75(1) ms to 7.1(1) ms.

E. Fibre noise cancellation

The fibre noise cancellation (FNC) for the 674 nm light uses an acousto-optical modulator (AOM) before the 15 m fibre to the optical table with Alice and Bob. We pick off light before this AOM, which is superimposed on a photodiode with light retro-reflected from the output facet of the fibre. We use this error signal to modify the rf input to the AOM[59]. All the experiments described in the main text were performed with this FNC turned on. The two-ion correlated measurements are insensitive to laser dephasing, as discussed in the text. While this is visible at long Ramsey durations, additional decoherence from magnetic field fluctuations further decreases the parity contrast. To unambiguously demonstrate the insensitivity to laser dephasing, we performed additional experiments with the FNC turned off, as shown in Fig. S6. Compared to the data in Fig. 2, at $T_R = 2.5$ ms we observe a complete loss in contrast of the single-ion signals due to laser dephasing, while the two-ion signals are essentially unchanged.

F. Duration of entanglement generation

We simultaneously excite each ion using a 422 nm pulse, and the spontaneously emitted photons are transmitted to the Bell state analyser where a coincident detection of a pair of photons projects the ions into an entangled state. As we only detect a small fraction of the emitted photons, the entanglement generation is probabilistic and has a variable duration. We note that, because the entanglement is heralded, all events are used without any post-selection. Each attempt has a duration of 1 μs, with 250 μs of laser cooling after every 1000 attempts. For the data in this work, the mean entanglement generation duration is about 9 ms. We plot the histogram of entanglement generation durations for a sample dataset in Fig. S7.

G. Single-ion and two-ion parity signal calculations

At the readout stage of the experimental sequence, we determine whether each ion was in the $|\downarrow\rangle$ or $|\uparrow\rangle$ state by recording its fluorescence. An ion in the state $|\downarrow\rangle$ is bright, while an ion in the $|\uparrow\rangle$ state is dark. For multiple repetitions at a given Ramsey duration, we can then determine the probability of each ion being in $|\downarrow\rangle$ ($P_\downarrow$) or $|\uparrow\rangle$ ($P_\uparrow$). The expectation value is $\langle\hat{\sigma}_{zi}\rangle = P_\uparrow - P_\downarrow = 1 - 2P_\downarrow$. To determine the parity for the two-ion measurements, we calculate $\langle\hat{\Pi}\rangle = \langle\hat{\sigma}_{z1}\hat{\sigma}_{z2}\rangle$. We use the same data to calculate the single-ion and the correlated unentangled two-ion parity signals using unentangled ions.

H. Entanglement-enhancement calculation

As given in Eq. 2, the single-shot frequency uncertainty for measuring $\Delta_i = \omega_L - \omega_i$ from a parity scan is

$$\delta\Delta_i = \frac{\delta\langle\hat{\Pi}_i\rangle}{C_i T_R},$$

where T_R is the Ramsey wait duration, C_i is the contrast of the single-ion parity fringe, and $\delta\langle\hat{\Pi}_i\rangle$ is the parity measurement uncertainty, which is ideally limited only by projection noise[39] and hence has a value of 1. From the single-ion experiments, the single-shot uncertainty in Δ_- is therefore

$$\delta\Delta_{-,s} = \frac{\delta\langle\hat{\Pi}_i\rangle}{T_R}\sqrt{\frac{1}{C_1^2}+\frac{1}{C_2^2}}. \tag{S2}$$

For the correlated two-ion measurements, the single-shot uncertainty in Δ_- is given by

$$\delta\Delta_{-,u|e} = \frac{\delta\langle\hat{\Pi}\rangle}{C T_R},$$

where C is now the contrast of the two-ion parity fringe. For $C_1 = C_2 = C$, using an entangled state thus gives a $\sqrt{2}$ reduction in the measurement uncertainty compared to single-atom measurements. Using simultaneous measurements of an unentangled two-ion state, C has a maximum value of $\frac{1}{2}$, which increases the single-shot uncertainty by a factor of 2 compared to the entangled state.

For Fig. 3, to obtain an error bar for the single-shot uncertainties and the entanglement enhancement, we only consider the uncertainty in the fitted parity contrasts and propagate the error accordingly.

I. Calibration for Stark shift measurement

To generate a differential shift between the two ions, we illuminate Alice's ion with a detuned 674 nm beam during the 15 ms Ramsey wait duration which gives an AC Stark shift. This beam is 35 MHz red-detuned from the $|S_{1/2}, m_j = -1/2\rangle \leftrightarrow |D_{5/2}, m_j = -3/2\rangle$ transition and has a power of $\sim 20\,\mu$W. The calibration data for the frequency shift measurement in Fig. 4 is shown in Fig. S8. The fitted Ramsey fringes allow us to convert a change in the parity signal to a frequency shift.

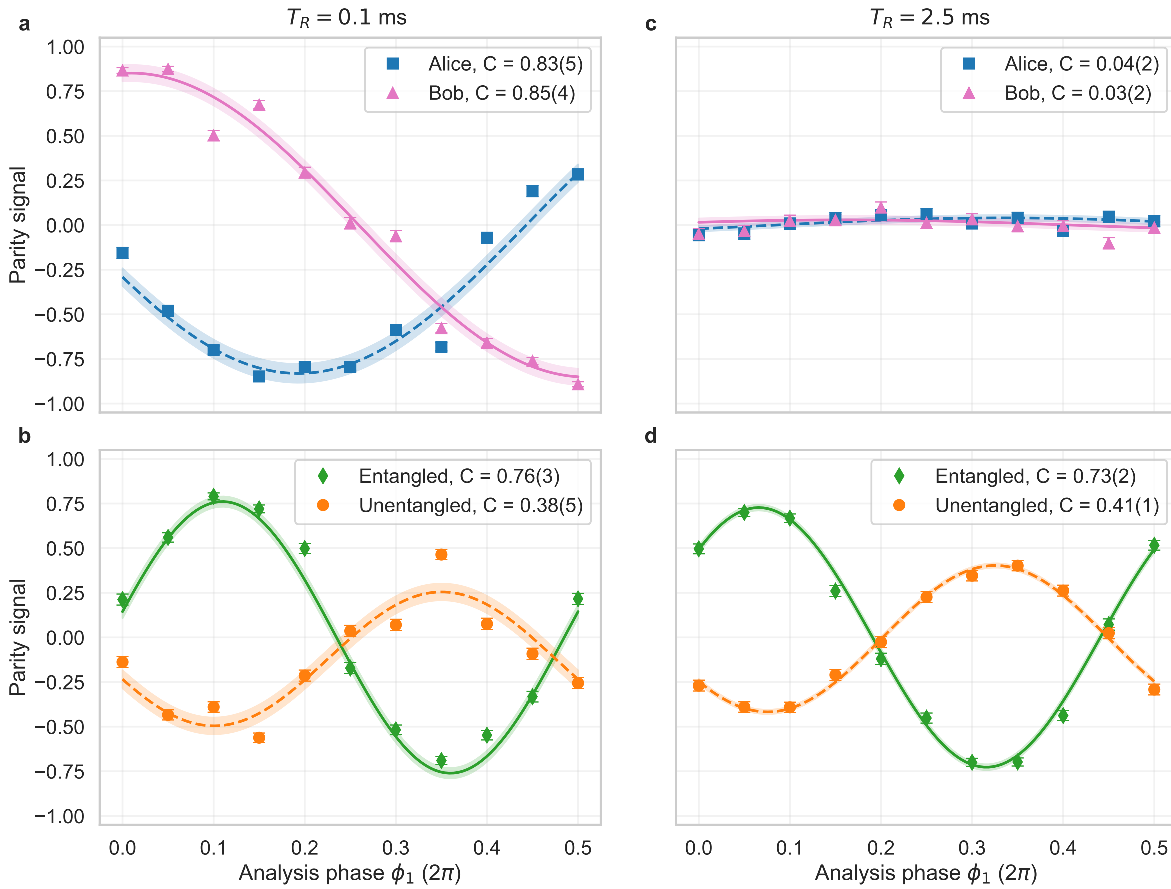

FIG. S6: Comparison of parity fringes with fibre noise cancellation (FNC) turned off, with and without entanglement, at Ramsey durations of 0.1 ms and 2.5 ms. We scan the analysis phase $\phi_1 = -\phi_2$ from 0 to π. We plot the single-ion data for each of Alice (blue squares) and Bob (pink triangles), and the two-ion data with (green diamonds) and without (orange circles) entanglement. (a) and (b) correspond to a Ramsey duration of 0.1 ms, while (c) and (d) correspond to a Ramsey duration of 2.5 ms. At 2.5 ms, qubit decoherence is minimal; the decoherence of the single-ion signals is primarily from laser dephasing, whilst the two-ion signals show no decrease in contrast. The shaded regions show the 68% confidence intervals of the best fit lines.

J. Effect of laser dephasing on parity signal

For the two-ion parity data in Fig. S2, we plot the error in the fitted contrasts and the value of the y-offset for the unentangled ions in Fig. S9. For the data in Fig. 4, we chose a Ramsey duration of 15 ms. At this duration, the y-offset was close to zero, but there was still some contribution to the fitted contrast error due to laser dephasing. However, at longer durations the overall contrast for both the entangled and unentangled ions had decayed further due to qubit frequency fluctuations.

[19] Stephenson, L. J. *et al.* High-Rate, High-Fidelity Entanglement of Qubits Across an Elementary Quantum Network. *Phys. Rev. Lett.* **124**, 110501 (2020).
[39] Itano, W. M. *et al.* Quantum projection noise: Population fluctuations in two-level systems. *Phys. Rev. A* **47**, 3554 (1993).
[57] Harmuth, H. F. Applications of Walsh functions in communications. *IEEE Spectr.* **6**, 82–91 (1969).
[58] Merkel, B. *et al.* Magnetic field stabilization system for atomic physics experiments. *Rev. Sci. Instrum.* **90**, 044702 (2019).
[59] Thirumalai, K. *High-fidelity mixed species entanglement of trapped ions*. Ph.D. thesis, University of Oxford (2019).

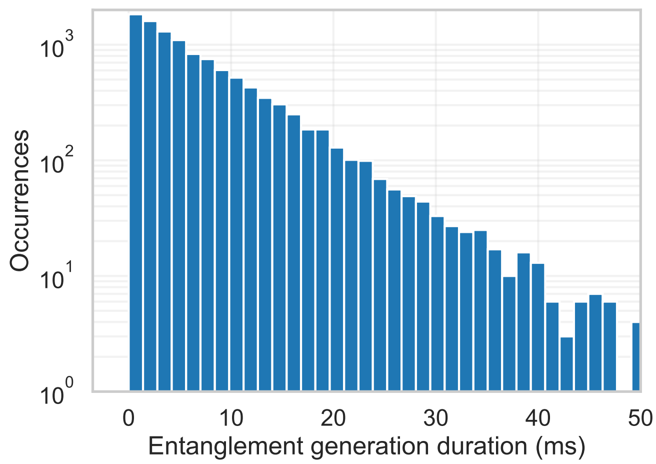

FIG. S7: Histogram of entanglement generation durations for a sample dataset. A total of 11000 attempts are plotted, with a mean duration of 9.2 ms.

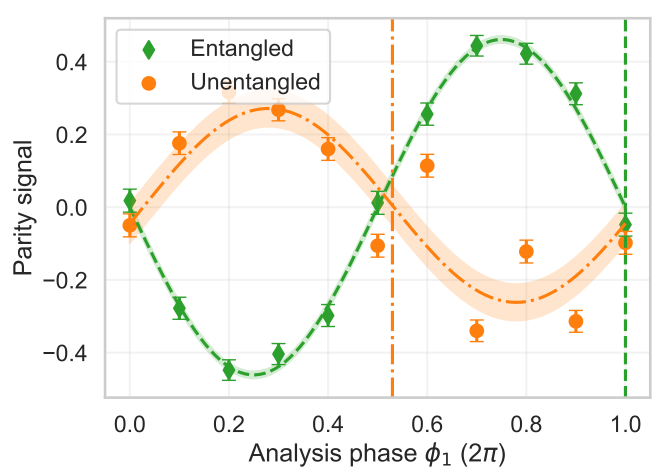

FIG. S8: Calibration data for the frequency difference measurement in Fig. 4a. For these data, $\phi_2 = 0$ and we only scan the value of ϕ_1 from 0 to 2π radians with no shift applied. From these data, we choose the phases at the steepest slopes indicated by the vertical lines for the unentangled (orange dash-dotted) and entangled (green dashed) states, respectively. The shaded regions indicate the 68% confidence intervals. As in Fig. 4a, the above-statistical scatter of the unentangled data points is evident.

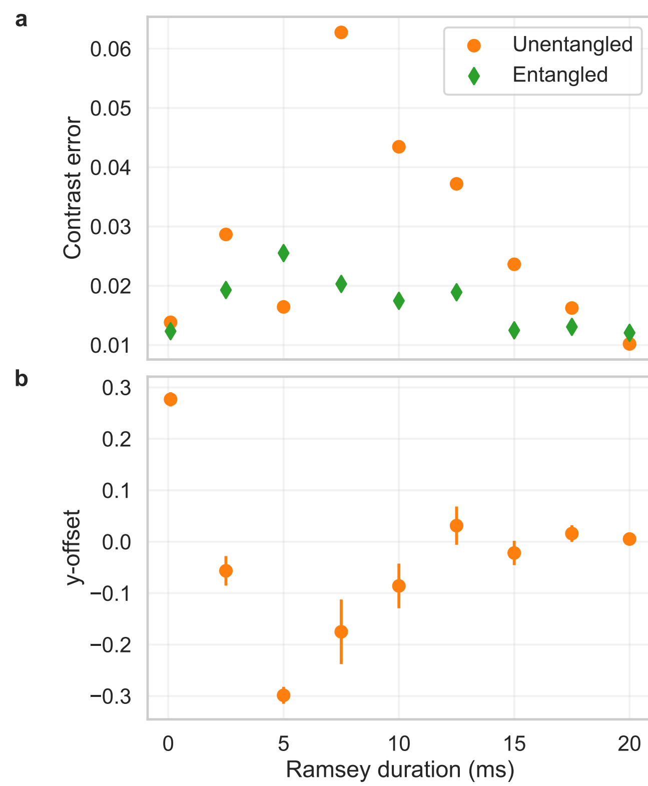

FIG. S9: Details of two-ion parity data from Fig. S2 for unentangled and entangled ions. a, For each value of the Ramsey duration, we plot the the error in the fitted value of contrast, C, from the parity signal for the two-ion data with (green diamonds) and without (orange circles) entanglement. Laser dephasing contributes to the error for the unentangled two-ion signal through the P_+ term (see Eq. 3), which is not present for the entangled-state parity. We suspect that this error increases because the Ramsey duration is similar to the timescale of the laser dephasing, which increases the uncertainty of the contrast due to the P_+ term. At longer durations, contributions from this term are reduced, and the magnitude of the error for the unentangled and entangled two-ion signals is similar at 20 ms. b, The parity signal for the unentangled two-ion signal is fitted with a y-offset to account for the P_+ term. We plot the value of this offset for all Ramsey durations. The y-offset reaches zero before the contributions of this term to the error have fully decayed.